ANTI-ALIASING FILTER FOR SUBPIXEL DOWN-SAMPLING BASED ON FREQUENCY ANALYSIS

Lu Fang, Ketan Tang, Oscar C. Au

Dept. of Electronic and Computer Engineering
Hong Kong Univ. of Sci. and Tech.
{fanglu, tkt, eeau}@ust.hk

Aggelos K. Katsaggelos

Dept. of EECS
Northwestern University
{aggk}@eecs.northwestern.edu

ABSTRACT

Nowadays, digital pictures are usually captured at very high resolution ranged up to 12 mega-pixels. Limited by low-resolution display, we have to shrink the image. Signal processing theory tells us that optimal decimation requires low-pass filtering with a suitable cut-off frequency followed by down-sampling. In doing so, we need to remove lots of details. Subpixel-based down-sampling, taking advantage of the fact that each pixel on a color LCD is actually composed of individual red, green, and blue subpixel stripes, can provide apparent higher resolution. In this paper, we use frequency domain analysis to explain what happens in subpixel-based down-sampling and why it is possible to achieve a higher apparent resolution. According to our frequency domain analysis and observation, the cut-off frequency of the low-pass filter for subpixel-based decimation can be effectively extended beyond the Nyquist frequency using a novel anti-aliasing filter. Experimental results verify that the proposed subpixel down-sampling scheme based on frequency analysis (SDSFA) can give superior results compared with existing pixel-based down-sampling methods.

1. INTRODUCTION

Subpixel rendering is a proven method capable of increasing the apparent resolution of fonts on an LCD display [1]. We typically think of a pixel as an inseparable region with a single color. However, the subpixels are visibly separated as shown in Fig. 1(a) when viewed at short distance with the help of a magnifying glass. Depending on the relative intensity of the components in a pixel, the apparent position or orientation of a line (such as the edge of a font) can be micro-shifted (i.e. shifted by a one or two subpixel width). Fig. 1(b) and 1(c) illustrate an example of whole pixel rendering and subpixel rendering by displaying the letter "m" [3], where subpixel rendering can provide better visual quality, with much less staircase artifacts.

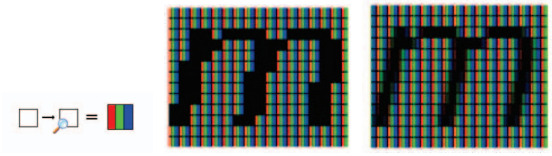

(a) (b) (c)

Fig. 1. (a) R, G, B subpixels (b) pixel rendering of character "m" (c) subpixel rendering of character "m".

In this paper, we are concerned about image down-sampling using subpixel techniques to achieve sharper images for small LCDs. Such a problem exists when a high resolution image or video is to be displayed on low resolution display terminals. For example, displaying high resolution images, ranged up to 12 mega-pixels, on computer LCD monitors, dedicated digital LCD photo-frames, or small LCD screens on mobile phones or PDAs, which have considerably lower resolutions.

For simplicity, we assume that an input high resolution image L (meaning $large$) of size $M \times N$ is to be down-sampled to a low resolution image S (meaning $small$) of size $m \times n$, to be displayed on a $m \times n$ device, where $M = 3m$ and $N = 3n$. (Note that if L is not of size $3m \times 3n$, i.e. the down-sampling ratio is not 3, we can use regular interpolation or decimation methods to resize L to be $3m \times 3n$.) A simple way called Direct Pixel-based Down-sampling (DPD) in this paper, is to perform simple down-sampling by selecting one out of every three pixels, as shown in Fig. 2(a). It can incur severe aliasing artifacts in regions with high spatial frequency, as verified in Fig. 2(b), where the grass is broken. An improved scheme is called Pixel-based Down-sampling with Anti-aliasing Filter (PDAF) in which an anti-aliasing filter is applied before direct pixel-based down-sampling to suppress aliasing artifacts. However, it smoothes the result at the price of blurring the image, as only the low frequency information can be retained in the process [5].

Since the number of individual reconstruction points in a LCD can be increased by three times by considering the subpixels, application of subpixel rendering in down-sampling schemes may lead to improvement in apparent resolution. Daly *et. al.* propose a simple subpixel-based down-sampling scheme which we call Direct Subpixel-based Down-sampling (DSD) in this paper [4]. DSD decimates the red, green, and blue components alternately in the horizontal direction. Let $(r_{i,j}, g_{i,j}, b_{i,j})$ be the $(i,j)^{th}$ pixel of S. The method copies the red, green, blue components (i.e., the three subpixels) of the pixel from three different pixels in L, such that $r_{i,j} = R_{3i-2,3j-2}$, $g_{i,j} = G_{3i-2,3j-1}$, $b_{i,j} = B_{3i-2,3j}$ as shown in Fig. 2(c), where $R_{3i-2,3j-2}$ is the red component of the $(3i-2, 3j-2)^{th}$ pixel of L and so on. A close examination of Fig. 2(d) reveals that DSD fills in the gaps of the grass making the grass continuous and sharp.

Unfortunately, direct application of subpixel approach to down-sampling may cause "color fringing" problem and result in very annoying artifacts, as shown in Fig. 2(d). In [2], Gibson uses a five-tap low-pass filter to smooth the result of the subpixel-based down-sampling. However, the low-pass filter relieves color fringing at the price of image blurring, and can be only adopted as an enhancement technique for achromatic image. Based on psychophysical experiments, [3] defines an error metric in frequency domain, and derives the filter coefficients by minimizing this metric. The filter in [3] is applied to achromatic (gray-scale) font rendering, which is the ba-

sis of Microsoft's ClearType system. In [4], an algorithm based on human visual system (HVS) is proposed to suppress visible chrominance aliasing.

In this paper, we attempt to use frequency analysis to analyze what happens in subpixel-based down-sampling and why it is possible to achieve higher apparent resolution. We then design novel anti-aliasing filter for DSD scheme based on our frequency domain analysis. The rest of the paper is organized as follows. In Section 2, we first analyze the frequency characteristics of DPD and DSD. Since DSD cause color fringing artifacts, we design novel anti-aliasing filter for DSD based on our frequency domain analysis. Experimental results are described in Section 3. Finally, Section 4 concludes the paper.

2. PROPOSED SUBPIXEL DOWN-SAMPLING BASED ON FREQUENCY ANALYSIS (SDSFA)

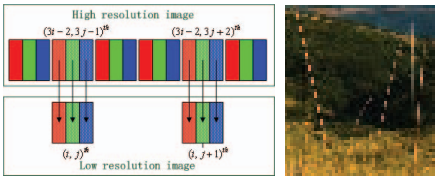

(a) DPD (b)

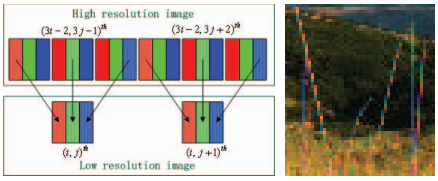

(c) DSD (d)

Fig. 2. (a) Direct Pixel-based Down-sampling (DPD) (b) magnified result of DPD, where "grass" is broken due to aliasing artifacts (c) Direct Subpixel-based Down-sampling (DSD) (d) magnified result of DSD, where "grass" is smooth but has color fringing artifacts.

To better understand the spatial multiplexing of RGB components of a DSD image, we define an auxiliary image L′ of size $M \times N$ and we use $(R'_{i,j}, G'_{i,j}, B'_{i,j})$ to represent the $(i,j)^{th}$ pixel of L′. We define the red component of L′ such that $R'_{i,j} = R_{i,j}$ for $i = 3i' - 2$ and $j = 3j' - 2$ for all possible (i', j'), and $R'_{i,j} = 0$ elsewhere, such that

$$R'_{i,j} = \begin{cases} R_{i,j}, & \text{for } i = 3i' - 2, j = 3j' - 2, \\ & i' = 1, \cdots, m,\ j' = 1, \cdots, n \\ 0, & \text{otherwise} \end{cases} \tag{1}$$

Effectively, out of every 3×3 sub-matrix of L′, one R' value is copied from L and the other eight are zero. Similarly, we define $G'_{i,j} = G_{i,j}$ for $i = 3i' - 2, j = 3j' - 1$, and $B'_{i,j} = B_{i,j}$ for $i = 3i' - 2, j = 3j'$, and zero elsewhere. As such, if DSD is applied to either L or L′, the same small image S will be obtained. We define the auxiliary luminance component $I(i,j)$ for the $(i,j)^{th}$ pixel as $I(i,j) = \frac{1}{3}(R'_{i,j} + G'_{i,j} + B'_{i,j})$,

$$\begin{aligned} I_{DSD}(i,j) &= \tfrac{1}{3}(R'_{i,j} + G'_{i,j} + B'_{i,j}) \\ &= \tfrac{1}{3}(R_{i,j}\Delta^R_{DSD} + G_{i,j}\Delta^G_{DSD} + B_{i,j}\Delta^B_{DSD}) \\ &= \textstyle\sum_p C^p(i,j)\Delta^p_{DSD}(i,j) \end{aligned} \tag{2}$$

where

$$\begin{aligned} \Delta^R_{DSD}(i,j) &= \begin{cases} 1, & \text{for } i = 3i' - 2, j = 3j' - 2 \\ 0, & \text{otherwise} \end{cases} \\ &= \tfrac{4}{9}\left(\tfrac{1}{2} + cos\tfrac{2\pi(i-2)}{3}\right)\left(\tfrac{1}{2} + cos\tfrac{2\pi(j-1)}{3}\right) \end{aligned} \tag{3}$$

and

$$\begin{aligned} \Delta^G_{DSD}(i,j) &= \tfrac{4}{9}\left(\tfrac{1}{2} + cos\tfrac{2\pi(i-2)}{3}\right)\left(\tfrac{1}{2} + cos\tfrac{2\pi(j-2)}{3}\right) \\ \Delta^B_{DSD}(i,j) &= \tfrac{4}{9}\left(\tfrac{1}{2} + cos\tfrac{2\pi(i-2)}{3}\right)\left(\tfrac{1}{2} + cos\tfrac{2\pi j}{3}\right) \end{aligned} \tag{4}$$

are the RGB modulation functions, and $C^p(i,j)$ are the three color components of L (R, G or B for p = 1, 2, or 3). The Fourier transform of I_{DSD} is

$$\widehat{I}_{DSD}(u,v) = \sum_p \widehat{C}^p(u,v) * \widehat{\Delta}^p_{DSD}(u,v) \tag{5}$$

where $\widehat{\cdot}$ represents the Discrete Time Fourier transform (with zero padding outside the support for I_{DSD} and Δ^p_{DSD} and $*$ is the convolution operator.

As the three RGB modulation functions in (3) and (4) are based on the cosine function, their Fourier transforms are expressed as Diracs,

$$\begin{aligned} &\widehat{\Delta}^R_{DSD}(u,v) \\ &= \tfrac{1}{9}\begin{pmatrix} a_1a_2\delta(u+\frac{1}{3}, v+\frac{1}{3}) + a_2\delta(u, v+\frac{1}{3}) + a_2^2\delta(u-\frac{1}{3}, v+\frac{1}{3}) \\ +a_1\delta(u+\frac{1}{3}, v) + \delta(u,v) + a_2\delta(u-\frac{1}{3}, v) \\ +a_1^2\delta(u+\frac{1}{3}, v-\frac{1}{3}) + a_1\delta(u, v-\frac{1}{3}) + a_1a_2\delta(u-\frac{1}{3}, v-\frac{1}{3}) \end{pmatrix} \\ &= \tfrac{1}{9}\begin{bmatrix} \delta(u+\frac{1}{3}) \\ \delta(u) \\ \delta(u-\frac{1}{3}) \end{bmatrix}^T \begin{bmatrix} a_1a_2 & a_1 & a_1^2 \\ a_2 & 1 & a_1 \\ a_2^2 & a_2 & a_1a_2 \end{bmatrix} \begin{bmatrix} \delta(v+\frac{1}{3}) \\ \delta(v) \\ \delta(v-\frac{1}{3}) \end{bmatrix} \end{aligned} \tag{6}$$

where $a_1 = e^{-j\frac{2\pi}{3}}$, $a_2 = e^{j\frac{2\pi}{3}}$. Similarly, we can compute the Fourier transform of Δ^G_{DSD} and Δ^B_{DSD}. We then represent them in a matrix form,

$$\begin{cases} \widehat{\Delta}^R_{DSD}(u,v) = \frac{1}{9}\mathbf{\Delta}(\mathbf{u})^T \begin{bmatrix} a_1a_2 & a_1 & a_1^2 \\ a_2 & 1 & a_1 \\ a_2^2 & a_2 & a_1a_2 \end{bmatrix} \mathbf{\Delta}(\mathbf{v}) \\ \widehat{\Delta}^G_{DSD}(u,v) = \frac{1}{9}\mathbf{\Delta}(\mathbf{u})^T \begin{bmatrix} a_1^2 & a_1 & a_1a_2 \\ a_1 & 1 & a_2 \\ a_1a_2 & a_2 & a_2^2 \end{bmatrix} \mathbf{\Delta}(\mathbf{v}) \\ \widehat{\Delta}^B_{DSD}(u,v) = \frac{1}{9}\mathbf{\Delta}(\mathbf{u})^T \begin{bmatrix} a_1 & a_1 & a_1 \\ 1 & 1 & 1 \\ a_2 & a_2 & a_2 \end{bmatrix} \mathbf{\Delta}(\mathbf{v}) \end{cases} \tag{7}$$

where $\mathbf{\Delta}(\mathbf{u})^T = [\delta(u+\frac{1}{3}), \delta(u), \delta(u-\frac{1}{3})]$ and $\mathbf{\Delta}(\mathbf{v})^T = [\delta(v+\frac{1}{3}), \delta(v), \delta(v-\frac{1}{3})]$.

Rewriting (5) with (7), and considering the relationship between a_1 and a_2,

$$a_1a_2 = 1,\ a_1^2 = a_2,\ a_2^2 = a_1. \tag{8}$$

we can obtain,

$$\begin{aligned} &\widehat{I}_{DSD}(u,v) = \tfrac{1}{3}\mathbf{1}_3^T \\ &\begin{bmatrix} a_1\hat{C}_2(u+\frac{1}{3}, v+\frac{1}{3}) & a_1\hat{Y}(u+\frac{1}{3}, v) & a_1\hat{C}_1(u+\frac{1}{3}, v-\frac{1}{3}) \\ \hat{C}_2(u, v+\frac{1}{3}) & \hat{Y}(u,v) & \hat{C}_1(u, v-\frac{1}{3}) \\ a_2\hat{C}_2(u-\frac{1}{3}, v+\frac{1}{3}) & a_2\hat{Y}(u-\frac{1}{3}, v) & a_2\hat{C}_1(u-\frac{1}{3}, v-\frac{1}{3}) \end{bmatrix} \mathbf{1}_3 \end{aligned} \tag{9}$$

where

$$\begin{cases} \widehat{Y}(u,v) = \frac{1}{3}(\hat{R}(u,v) + \hat{G}(u,v) + \hat{B}(u,v)) \\ \widehat{C}_1(u,v) = \frac{1}{3}(a_1\hat{R}(u,v) + a_2\hat{G}(u,v) + \hat{B}(u,v)) \\ \widehat{C}_2(u,v) = \frac{1}{3}(a_2\hat{R}(u,v) + a_1\hat{G}(u,v) + \hat{B}(u,v)) \end{cases} \tag{10}$$

To compare the difference between DSD and DPD, we define the corresponding I_{DPD} similar to (2) of which the three RGB modulation functions are Δ^p_{DPD} as defined in (11). Note that the Δ^p_{DPD} are identical for R, G and B color components in DPD.

$$\begin{aligned} &\Delta^R_{DPD}(i,j) = \Delta^G_{DPD}(i,j) = \Delta^B_{DPD}(i,j) \\ &= \tfrac{4}{9}\left(\tfrac{1}{2} + cos\tfrac{2\pi(i-2)}{3}\right)\left(\tfrac{1}{2} + cos\tfrac{2\pi(j-2)}{3}\right) \end{aligned} \tag{11}$$

The Fourier transform of I_{DPD} is given by

$$\widehat{I}_{DPD}(u,v) = \tfrac{1}{3}\mathbf{1}_3^T \begin{bmatrix} a_2\hat{Y}(u+\frac{1}{3},v+\frac{1}{3}) & a_1\hat{Y}(u+\frac{1}{3},v) & \hat{Y}(u+\frac{1}{3},v-\frac{1}{3}) \\ a_1\hat{Y}(u,v+\frac{1}{3}) & \hat{Y}(u,v) & a_2\hat{Y}(u,v-\frac{1}{3}) \\ \hat{Y}(u-\frac{1}{3},v+\frac{1}{3}) & a_2\hat{Y}(u-\frac{1}{3},v) & a_1\hat{Y}(u-\frac{1}{3},v-\frac{1}{3}) \end{bmatrix} \mathbf{1}_3 \tag{12}$$

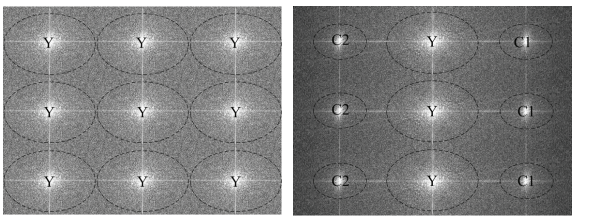

(a) DPD (b) DSD

Fig. 3. (a) Frequency spectrum of $\widehat{I}_{DPD}$ (b) frequency spectrum of $\widehat{I}_{DSD}$.

Fig. 3 shows the magnitude of $\widehat{I}_{DSD}$ in (9) and $\widehat{I}_{DPD}$ in (12). We clearly see nine replicated spectrums situated at $u \in \{-\frac{1}{3},\ 0,\ \frac{1}{3}\}$ and $v \in \{-\frac{1}{3},\ 0,\ \frac{1}{3}\}$ in each of $\widehat{I}_{DSD}$ and $\widehat{I}_{DPD}$ corresponding to the nine Diracs locations. Examining Fig. 3(a), all the nine replicated spectrums of $\widehat{I}_{DPD}$ are $\hat{Y}$ with equal magnitude, since the magnitude of a_1 and a_2 is 1 in (12). The magnitude of $\widehat{I}_{DSD}$ is obviously different from that of $\widehat{I}_{DPD}$. While the three center replicated spectrums of $\widehat{I}_{DSD}$ are $\hat{Y}$, the three on the right are $\hat{C}_1$ and the three on the left are $\hat{C}_2$ corresponding to (9). The horizontal shifting of sampling locations of the three colors in DSD leads to the replacement of $\hat{Y}$ by $\hat{C}_1$ and $\hat{C}_2$ on the two sides of $\widehat{I}_{DSD}$. And it appears that $\hat{C}_1$ and $\hat{C}_2$ are significantly different from $\hat{Y}$.

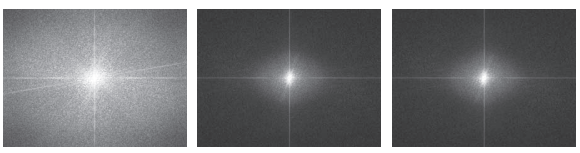

(a) Y (b) C1 (c) C2

Fig. 4. (a) Frequency spectrum of Y component (b) frequency spectrum of C_1 component (c) frequency spectrum of C_2 component.

To examine the difference between $\hat{C}_1$, $\hat{C}_2$ and $\hat{Y}$, we compare the magnitude of $\hat{Y}$, $\hat{C}_1$ and $\hat{C}_2$ as shown in Fig. 4. All three have more energy at low frequency than high frequency, as expected. Although $\hat{C}_1$, $\hat{C}_2$ and $\hat{Y}$ are weighted sums of $\hat{R}$, $\hat{G}$ and $\hat{B}$ according to (10), their magnitude in Fig. 4 can be quite different.

Both $\hat{C}_1$ and $\hat{C}_2$ appear to have more compact spectrums than $\hat{Y}$. This can be explained as follows. Any signal such as R can be decomposed into a low-frequency term R_l and a high frequency term R_h. It is well known that the high frequency components of different colors tend to be similar [6], i.e. $\hat{R}_h(u,v) \approx \hat{G}_h(u,v) \approx \hat{B}_h(u,v)$. This implies

$$\begin{aligned} \widehat{C}_1(u,v) &= \tfrac{1}{3}[a_1\hat{R}(u,v) + a_2\hat{G}(u,v) + \hat{B}(u,v)] \\ &= \tfrac{1}{3}[a_1(\hat{R}_l + \hat{R}_h) + a_2(\hat{G}_l + \hat{G}_h) + (\hat{B}_l + \hat{B}_h)] \\ &\approx \tfrac{1}{3}[(a_1\hat{R}_l + a_2\hat{G}_l + \hat{B}_l) + (a_1 + a_2 + 1)\hat{G}_h] \\ &= \tfrac{1}{3}[a_1\hat{R}_l(u,v) + a_2\hat{G}_l(u,v) + \hat{B}_l(u,v)] \end{aligned} \tag{13}$$

since $a_1 + a_2 + 1 \equiv 0$. This means that $\hat{C}_1$ is mainly a low frequency signal, with very little high frequency energy. A similar argument applies to $\hat{C}_2$. With the low-frequency nature of $\hat{C}_1$ and $\hat{C}_2$, the horizontal overlap in DSD between the center $\hat{Y}$ and the $\hat{C}_1$ on the right and the $\hat{C}_2$ on the left are significantly lower than the horizontal overlap in DPD among the $\hat{Y}$.

Let $A = \frac{1}{3}$ be both the horizontal and vertical shifts of the replicated spectrums such that, for DSD, $\hat{Y}$ is located at $(0, A)$, $(0, 0)$ and $(0, -A)$, $\hat{C}_1$ at (A, A), $(A, 0)$ and $(A, -A)$, and $\hat{C}_2$ at $(-A, A)$, $(-A, 0)$ and $(-A, -A)$. For DPD, it is $\hat{Y}$ at the same 9 locations. Let f_c^H and f_c^V be the horizontal and vertical cut-off frequency for different down-sampling methods. For DPD, the horizontal and vertical cut-off frequency to prevent aliasing should be $f_c^H = f_c^V = \frac{A}{2}$. For DSD, as the three vertical replicated spectrum are identical, the vertical cut-off frequency should be the same as DPD with $f_c^V = \frac{A}{2}$. While with the smaller amount of horizontal overlap in DSD, it is possible for us to use a higher horizontal cut-off frequency $f_c^H \geq \frac{A}{2}$ to retain more of the signal details in $\hat{Y}$. Recall that the main energy of $\hat{Y}$, $\hat{C}_1$ and $\hat{C}_2$ is highly concentrated in center, we then calculate 99% of the total energy for each of $\hat{Y}$, $\hat{C}_1$ and $\hat{C}_2$, using the ratio of the 99%-energy to further determine the f_c^H,

$$f_c^H = \tfrac{k}{k+1}A, \quad f_c^V = \tfrac{A}{2} \tag{14}$$

where $k = min(\sqrt{\frac{E_Y}{E_{C1}}}, \sqrt{\frac{E_Y}{E_{C2}}})$.

3. IMPLEMENTATION AND RESULTS

In this section, we simulate the proposed subpixel down-sampling based on frequency analysis (SDSFA), and six test images shown in Fig. 5 are used. We will compare our method with PDAF, which is the standard pixel-based down-sampling method. In particular, we examine their luminance apparent resolution and chrominance distortion. Here we choose YUV color space [7].

To examine the luminance apparent resolution, we firstly compute the average of directional high-frequency "energy" by convolving a 1-D high pass filter in four directions, $E(x) = \frac{1}{4}\sum_{k=1}^{4} ||H_a^k * x||_2^2$, where H_a^k is 1-D high pass filter $a = [1\ -1]$ and k represents horizontal, vertical, diagonal and anti-diagonal directions. We further define P_a as the ratio of H_a^k-filtered x to H_a^k-filtered DSD. Here we choose DSD as a reference for the sake of comparison because it gives rather sharp resultant images with much high frequency details. By definition, P_a is positive number. A higher value indicates

Fig. 5. Source images used in experiment.

that there is more luminance high frequency energy which suggests higher apparent luminance resolution.

$$P_a \triangleq \frac{E(x)}{E(\text{DSD})} = \frac{\sum_{k=1}^{4} ||H_a^k * x||_2^2}{\sum_{k=1}^{4} ||H_a^k * \text{DSD}||_2^2}, \quad (15)$$

As for chrominance measure, we observe that PDAF typically does not give chrominance distortion. Therefore, for any image x to be measured, we choose the chrominance components of PDAF as the reference to compute PSNR_U and PSNR_V.

$$\text{PSNR}_\text{U} \triangleq 10log_{10}(\frac{255^2}{\text{MSE}_\text{U}}),\ \text{MSE}_\text{U} \triangleq \frac{||\text{U}_x - \text{U}_\text{PDAF}||_2^2}{MN} \quad (16)$$

where U_PDAF and U_x are the U components of PDAF and x respectively. The PSNR_V is defined similarly.

Table 1. Objective measure for luminance sharpness.

	P_a		P_b	
Image	PDAF	SDSFA	PDAF	SDSFA
1	0.825	1.001	0.811	0.961
2	0.735	0.974	0.739	0.943
3	0.795	0.953	0.778	0.942
4	0.792	0.974	0.778	0.948
5	0.868	1.000	0.835	0.979
6	0.787	0.989	0.705	0.924
ave	0.800	0.982	0.774	0.950

Table 2. Objective measure for chrominance distortion.

	PSNR_U		PSNR_V	
Image	DSD	SDSFA	DSD	SDSFA
1	28.0	31.4	28.2	31.9
2	29.6	33.4	29.8	33.2
3	28.7	33.2	29.7	34.4
4	26.6	32.4	26.2	32.9
5	27.7	29.7	27.5	30.0
6	30.6	33.5	30.8	34.0
ave	28.5	32.3	28.7	32.7

While we are not sure whether filter $a = [1 - 1]$ or filter $b = [1 - 21]$ is better for measuring luminance sharpness, we show both P_a and P_b values in Table 1, and both filters give consistent results for our performance comparison. Tables 1 shows that the values P_a and P_b of the proposed SDSFA are significantly larger than PDAF, suggesting that SDSFA retains more high frequency details than PDAF. In other words, SDSFA tends to give higher apparent luminance resolution, leading to clearer and sharper down-sampled images as verified in Fig. 6. From Table 2, we observe that the PSNR_U and PSNR_V of DSD are about $3 - 4$ dB lower than SDSFA which suggests that SDSFA can suppress chrominance distortion effectively.

4. CONCLUSION

In this paper, we use frequency analysis to explain what happens in subpixel-based down-sampling and why this is possible to provide higher apparent resolution. According to our frequency analysis, we design novel anti-aliasing filter for DSD. Experimental results verify that the proposed method outperforms existing standard pixel-based down-sampling method, leading to sharper and clearer results.

5. ACKNOWLEDGMENT

This work has been supported in part by the Research Grants Council (GRF 610109) and the Innovation and Technology Commission (GHP/048/08) of Hong Kong, China.

6. REFERENCES

[1] E. Brown, C. H. Brown, et. al., “Co-Optimization of Color AMLCD Subpixel Architecture and Rendering Algorithms", *SID Digest*, pp. 172ÍC175, 2002.

[2] S. Gibson, “ Sub-Pixel Font Rendering Technology", *from http://www.grc.com/cleartype.htm*.

[3] J. C. Platt, “Optimal Filtering for Patterned Displays", *IEEE Signal Processing Letters*, Vol. 7, No. 7, pp. 179-181, July 2000.

[4] S. J. Daly, et. al., “Methods and Systems for Improving Display Resolution in Images using Sub-pixel Sampling and Visual Error Filtering", *United States Patent*, US 6,608,632 B2, Aug. 2003.

[5] P. S. R. Diniz, E. A. B. D. Silva, and S. L. Netto (2002), *Digital Signal Processing: System Analysis and Design*, Cambridge University Press., ISBN 0521781752.

[6] Lian, N. X. and Chang, L. and Tan, Y. P. and Zagorodnov, V., “ Adaptive filtering for color filter array demosaicking”, *IEEE Transactions on Image Processing*, Vol. 16, No. 10, pp. 2515-2525, 2007.

[7] ITU, recommendation ITU-R BT.601-5, 1995.

(a) PDAF (b) Proposed

Fig. 6. Experimental results, (a) PDAF (b) Proposed.